Branch intensities and oscillator strengths for the Herzberg absorption systems in oxygen

DAVID L. HUESTIS,[1] RICHARD A. COPELAND, KAREN KNUTSEN, AND TOM G. SLANGER
Molecular Physics Laboratory, SRI International, Menlo Park, CA 94025, U.S.A.

AND

RIENK T. JONGMA, MAARTEN G.H. BOOGAARTS, AND GERARD MEIJER
Department of Molecular and Laser Physics, University of Nijmegen, Toernooiveld, 6525 ED Nijmegen, The Netherlands

Received April 6, 1994
Accepted July 5, 1994

This paper is dedicated to Dr. Gerhard Herzberg on the occasion of his 90th birthday

We report two complementary experimental investigations of the absorption spectrum of molecular oxygen between 243 and 258 nm. In the first experiment, excitation of O_2 is inferred by detecting oxygen atoms resulting from chemical reaction. In the second experiment, absorption by O_2 is observed directly by cavity ring-down spectroscopy. Absorption strengths for the Herzberg I ($A^3\Sigma_u^+ \leftarrow X^3\Sigma_g^-$), Herzberg II ($c^1\Sigma_u^- \leftarrow X^3\Sigma_g^-$), and Herzberg III ($A'^3\Delta_u \leftarrow X^3\Sigma_g^-$) band systems are modeled with the DIATOM spectral simulation computer program using the best available branch intensity formulas. Absolute oscillator strengths are derived for all three systems and compared with values in the literature.

Nous présentons deux investigations complémentaires du spectre d'absorption de l'oxygène moléculaire entre 243 et 258 nm. Dans la première expérience, l'excitation de O_2 est inférée par la détection d'atomes d'oxygène provenant de réactions chimiques. Dans la seconde, l'absorption par O_2 est observée directment dans une cavité ("cavity ring-down spectroscopy"). Les forces d'absorption pour les systèmes de bandes Herzberg I ($A^3\Sigma_u^+ \leftarrow X^3\Sigma_g^-$), Herzberg II ($c^1\Sigma_u^- \leftarrow X^3\Sigma_g^-$) et Herzberg III ($A'^3\Delta_u \leftarrow X^3\Sigma_g^-$) sont modélisées avec le programme DIATOM de simulation spectrale par ordinateur, en utilisant les meilleures formules disponibles pour les intensités des branches. Les forces d'oscillateurs absolues sont calculées et comparées avec les valeurs rapportées dans la littérature.

[Traduit par la rédaction]

Can. J. Phys. **72**, 1109 (1994)

1. Introduction

The forbidden transitions of molecular oxygen play conspicuous roles in understanding the earth's atmosphere [1–5] and offer special challenges to the spectroscopist. Among the six spectroscopically known bound states that result from association of ground state oxygen atoms, $X^3\Sigma_g^-$, $a^1\Delta_g$, $b^1\Sigma_g^+$, $c^1\Sigma_u^-$, $A'^3\Delta_u$, and $A^3\Sigma_u^+$, there are 15 possible radiative transitions, all of which are forbidden. Eight of these transitions have been observed (see Table 1), all terminating on either the ground or the first excited state. All of the five transitions terminating on the ground state are associated with the work of Gerhard Herzberg, and three carry his name in their designation.

TABLE 1. Forbidden transitions in O_2

	$X^3\Sigma_g^-$	$a^1\Delta_g$
$A^3\Sigma_u^+$	Herzberg I	(Unobserved)
$A'^3\Delta_u$	Herzberg III	Chamberlain
$c^1\Sigma_u^-$	Herzberg II	Richards–Johnson
$b^1\Sigma_g^+$	Atmospheric	Noxon
$a^1\Delta_g$	Infrared-atmospheric	

1.1. Line positions and branch intensities

The transition $A^3\Sigma_u^+ - X^3\Sigma_g^-$ in O_2 has a long and distinguished history, beginning with its discovery by Herzberg in 1932 [6], which in turn led to its designation of "Herzberg I," being the first of the three 240–260 nm absorption systems in O_2 that he studied. As remarked by Present [7], the appearance of this spectrum is unusual in that at moderate resolution it consists of three Q-form branches, of approximate relative strength of 2:1:2. As the resolution and sensitivity are improved [8, 9], the three strong Q-form branches are resolved into five branches of nearly equal strength, plus one weak satellite Q-form branch on each side, in addition to three weak S-form and three weak O-form branches on the blue and red sides, respectively.

In the first attempt to calculate the branch strengths for O_2 $A^3\Sigma_u^+ - X^3\Sigma_g^-$, Present [7] considered the possibility of mixing of either the upper or lower state with a $^3\Pi$ state by either spin-orbit or rotational coupling. Choosing one of these two coupling mechanisms gives an intensity distribution with some strong Q-form branches, and weaker O-form and S-form branches, but neither is satisfactory [8]. In our earlier paper [10] on the $A'^3\Delta_u \rightarrow a^1\Delta_g$ transition, we showed a simulation of the $A^3\Sigma_u^+ \rightarrow X^3\Sigma_g^-$ transition that included a new source of transition probability, spin-orbit mixing of $A^3\Sigma_u^+$ with the well-known $B^3\Sigma_u^-$ state, in addition to spin-orbit mixing of an unspecified $^3\Pi_g$ state with $X^3\Sigma_g^-$. That simulation was a significant improvement over the previous attempts, but quantitative results are obtained only by including all three perturbations. Even though the rotational mixing with the $^3\Pi$ state makes a minor contribution to the total transition probability, its alternate constructive and destructive interference with the stronger spin-orbit-induced contributions has a profound influence on the relative strengths of the branches. Our work was described in a conference presentation [11]. Similar ideas have been developed and documented by Lewis and Gibson [12], modified by Cann and Nicholls [13], and applied qualitatively to the Herzberg I transition.

[1]Author to whom correspondence may be addressed.

Printed in Canada / Imprimé au Canada

The $c^1\Sigma_u^- - X^3\Sigma_g^-$ transition in O_2 was discovered in 1953 by Herzberg [14], and is called "Herzberg II." His absorption spectra showed transitions to the excited-state vibrational levels that we would now label $v' = 6$–11 [15]. The more recent absorption studies of Ramsay [16] have characterized a wider range of v' levels, from 1 to 16. Emission from $v' = 0$–2 to $v'' = 5$–13 has been observed in the laboratory [15, 17–19], from $v' = 4$–7 to $v'' = 3$–8 in the terrestrial nightglow [4], and from $v' = 0$ to $v'' = 5$–13 in the nightglow of Venus [17, 20, 21]. Four rotational branches are observed, named ${}^RR$, ${}^RQ$, ${}^PQ$, and ${}^PP$. Only one contribution to the transition moment is known, making the intensity formulas well defined, and in reasonable agreement with experiment [10].

The $A'^3\Delta_u - X^3\Sigma_g^-$ transition in O_2 also was discovered in absorption in 1953 by Herzberg [14], and is called "Herzberg III." To our knowledge the only report of emission in the gas phase on this transition is that of Slanger [18]. In analogy with a $^3\Pi - {}^3\Sigma^-$ transition, there are 27 rotational branches, 9 originating from each of the three Ω components of $A'^3\Delta_u$. Information on the relative intensities of these 27 branches is extremely limited. Kerr and Watson [22] used multiple spin-orbit and rotational contributions to fit a portion of the high-resolution absorption spectrum taken by Coquart and Ramsay [23]. We do not know of any published graphical spectra at rotational resolution showing the $A'^3\Delta_u - X^3\Sigma_g^-$ transition and thus do not have much experience in how well the Kerr and Watson formulas will do over a wide range of vibrational levels.

1.2. Oscillator strengths

Knowledge of the absorption cross sections and Einstein coefficients for the Herzberg transitions is important for a variety of atmospheric applications. Absorption of solar radiation in the so-called "Herzberg continuum" at wavelengths shorter than 243 nm is a significant source of oxygen atoms, and thus ozone, at lower altitudes. The concentrations of $A^3\Sigma_u^+$, $c^1\Sigma_u^-$, and $A'^3\Delta_u$ are inferred from their emission intensities. A principal objective is to monitor remotely the concentration of atomic oxygen in the upper atmosphere, the recombination of which is believed to be the major source of the Herzberg states. The Herzberg states have also been proposed as sources of $O(^1S)$, $O_2(b^1\Sigma_g^+)$, and vibrationally excited ozone.

Four kinds of primary information exist: (*i*) relative emission intensities for Herzberg I measured photographically by Degen and Nicholls in 1969 [24], (*ii*) integrated absorption cross section photographic measurements for the 7–0 (Hasson et al. [25]) and 4–0 through 11–0 (Hasson and Nicholls [26]) vibrational bands of Herzberg I, (*iii*) wavelength-resolved absorption cross section measurements for the Herzberg continuum (Herzberg I, II, and III, see Yoshino et al. [27] and references therein), and (*iv*) calculated transition moments from Klotz and Peyerimhoff [28].

The theoretical transition moments [28] have been used by Bates [29] to calculate Einstein coefficients for all three systems, Herzberg I, II, and III. Saxon and Slanger [30] used the theoretical transition moments to calculate the absorption cross section for the Herzberg continuum (calculated to be approximately 70% Herzberg I). Both of these works found that the calculated transition strengths are about 1.7 times larger than the best available experimental values [25, 26, 31]. For the absolute strengths of the Herzberg II and III transitions almost no usable experimental information is available in the literature.

1.3. Summary of the present work

Overall, only very limited data exist that can be used for quantitative investigation of branch intensities and oscillator strengths for the Herzberg bands. Until the experiments reported here, the only extensive "electrically" instead of "photographically" recorded spectrum was that of Wildt et al. [32] in which Herzberg band absorption is inferred indirectly by monitoring $b^1\Sigma_g^+ \rightarrow X^3\Sigma_g^-$ emission following collisional cascade.

We have performed two complementary experimental investigations of the strength of absorption by molecular oxygen between 243 and 258 nm. In the first experiment, performed at SRI, excitation of O_2 is inferred by detecting oxygen atoms resulting from subsequent chemical reaction, or photodissociation for $v' = 8$. This experiment provides relatively high spectral resolution and reliable relative branch intensities, but, being an indirect measurement, no absolute transition probabilities or relative transition strengths of the three systems.

In the second experiment, done at the University of Nijmegen, absorption by O_2 is observed directly by cavity ring-down spectroscopy. This experiment should provide absolute absorption strengths with potentially high spectral resolution and high sensitivity, but the rather broad-band laser used in these initial studies leads to lower resolution and some difficulties in data analysis due to non-Beer's-law behavior.

Absorption strengths for the Herzberg I, Herzberg II, and Herzberg III band systems are modeled with the DIATOM spectral simulation computer program (developed at SRI) using the best available branch intensity formulas. Absolute oscillator strengths are derived for all three systems and compared with values in the literature.

2. Experimental methods

2.1. Oxygen atom production

The collisional behavior of the O_2 Herzberg states in the upper atmosphere has long been a source of conjecture. For most altitudes, radiation is expected to be a minor loss process. We are conducting experiments to investigate the possibility that O_2 in $A^3\Sigma_u^+$, $A'^3\Delta_u$, or $c^1\Sigma_u^-$ states reacts with O_2 to form ozone. In the experiments described here the formation of ozone,

$$O_2^* + O_2 \rightarrow O_3 + O \qquad (1)$$

is inferred by detecting the O-atom reaction product using two-photon laser-induced fluorescence (LIF). In this paper we will use the intensity of the O-atom LIF signal as an indirect measure of the excitation probability, or absorption cross section, assuming that the O-atom yield is a slowly varying function of K. The kinetics and vibrational-level-dependent yield of O-atom production from $A^3\Sigma_u^+$ have been described elsewhere [33].

The "excitation" laser beam, consisting of the frequency-doubled output of a dye laser pumped by a frequency-tripled Nd:YAG laser operating at 10 Hz, excites O_2 at pressures of 8–14 Torr (1 Torr = 133.3 Pa) flowing slowly through the cell. The "detection" laser beam is the frequency-doubled output of an excimer-pumped dye laser, also operating at 10 Hz, and is counter-propagated to the first beam, and tuned to detect $O(^3P_2)$ via two-photon LIF at 225.7 nm [34, 35]. The resulting infrared fluorescence is monitored with a photomultiplier at right angles to laser propagation directions. Filters that pass light to the red of ~720 nm (Schott RG-665 and RG-715) are

used to discriminate against scattered light. The analog photomultiplier output is amplified and fed into a gated integrator averaging 10 samples, and collected using an A/D converter by a computer. Spectra are obtained by scanning the excitation laser. From fitting individual peaks we infer a spectral width of about 0.25 cm^{-1}. The two laser beams are focused into the center of the flow cell by 40 cm lenses, and are overlapped in space. By scanning the time delay between the laser pulses, the time evolution of the O-atom signal is measured. The spectra obtained in this work are taken at a time delay of 1 μs between the excitation and detection pulses to assure that the collisional production of O atoms has reached completion. Subsequent decay of the O-atom signal is slow, and is due to diffusion of the atoms out of the region of overlap of the two laser beams.

The energy of 225.7 nm O-atom detection laser photons is sufficient to dissociate O_2, and then probe the atoms generated. This produces a background signal to the two-laser experiment, but also provides a confirmation of resonance with the O-atom line. We normalize all spectra to the product of the excitation laser power times the O-atom detection laser power squared. Power dependence studies of the one-laser background O-atom signal show that the assumption of a squared power dependence for the two-photon LIF signal is reasonable. For large changes in the laser power the approximation to the square of the detection laser power has not been adequately examined, but this laser power typically fluctuates by less than 5% over the course of a scan, and so will have little effect upon relative transition intensities. We measure a linear power dependence of the signal with respect to the excitation laser (which fluctuates by ±15% during the course of a scan). The absolute signal intensities also are quite sensitive to the laser beam overlap, and can differ significantly between scans if the spatial overlap is adjusted, as is often the case.

Varying O-atom yields and significant vibrational-level dependence in kinetic behavior make it quite difficult to obtain absolute transition probabilities or even relative vibrational-band transition strengths from these spectra. However, the appearance of the spectra suggests either that rotational relaxation is more rapid than reaction with O_2 or that the O-atom yield is relatively independent of rotational level. In fact two additional mechanisms for O-atom production appear to be operating. For $v' = 11$, collisional dissociation provides a contribution, while for $v' = 8$, we observe two-photon resonance-enhanced photodissociation by the excitation laser. All of these processes appear to be relatively independent of the rotational level excited. Thus we will use the signal strengths within a single scan as an indication of the relative rotational branch intensities.

2.2. *Cavity ring-down spectroscopy*

Application of direct absorption techniques is advantageous in a variety of research fields, yielding both quantitative *absolute* concentrations as well as *absolute* frequency-dependent absorption cross sections. For these reasons absorption techniques are now undergoing a renaissance even in areas in which more sophisticated laser-based techniques are commonly applied. A drawback of direct absorption can be one of limited sensitivity. A small attenuation in transmitted light intensity has to be measured on top of a large background. One must be able to distinguish fluctuations in the light source intensity from variations in the sample absorption. Using continuous light sources, attenuations on the order of $10^{-4} - 10^{-5}$ can be measured. Pulsed light sources limit attenuations to values around $10^{-2} - 10^{-3}$ per pass.

Cavity Ring-Down Spectroscopy (CRDS) was proposed by O'Keefe and Deacon in 1988 [36] as an alternate way to perform direct absorption spectroscopy with pulsed light sources. By making repeated measurements of a single laser pulse bouncing between two high-reflectivity mirrors, the benefits of a long path length are achieved while circumventing the problems of intensity fluctuations in the light source. Recent CRDS studies [36–38] have demonstrated measurement of absorptions as low as 10^{-10} cm^{-1} in the visible where high-reflectivity mirrors ($R \geq 0.9999$) are available. Our work has emphasized extension of the CRDS technique into the ultraviolet [39, 40], even down to 200 nm. Around 250 nm, where no mirrors with reflectivity better than 0.997 are available, absorptions down to 10^{-7} cm^{-1} are readily detected.

Many of the techniques used in the present experiments are described in a recent publication [39]. The frequency-doubled output of a Nd:YAG laser (Spectra Physics GCR-150-10) is used to pump a dye laser (Spectra Physics PDL-3) operating on Fluorescein 548 dye. The dye laser output is frequency doubled and Raman shifted in 5 bar (1 bar = 100 kPa) of H_2, using a 200 cm focal-length lens, resulting in about 100 nJ of tunable uv radiation, with a Lorentzian line shape of about 0.5 cm^{-1} full-width at half-maximum. Typically 1% of this radiation is used in subsequent experiments.

The ring-down cavity consists of two identical 1 in. diameter plano-concave mirrors with a radius of curvature of 25 cm that have a high-reflectance KrF (248 nm) coating and a specified reflectivity, R, of greater than 0.995 in the 245–255 nm region (LaserOptik GmbH, Garbsen, Germany). The mirrors are placed 45.5 cm apart to form a highly stable optical cavity and to assure that the cavity mode spectrum is a quasi-continuum when the 2 mm diameter laser beam is coupled into the cavity through one of the end mirrors [39]. The time dependence of the transmitted laser intensity is monitored by a photomultiplier tube (PMT), placed directly behind the other cavity mirror to ensure that all the transverse cavity modes are collected with equal efficiency. The signal from the PMT is digitized on a digital oscilloscope with a 100 MHz sampling rate and a 10-bit vertical resolution (LeCroy 9430). The time histories at a fixed laser wavelength are summed into a 16 bit memory over a number of laser shots (typically 50), to improve the measurement statistics, and read out by a computer.

After the background is subtracted, the natural logarithm of the data is fit to a straight line. Dividing the slope of the line ($1/\tau$) by the speed of light gives the apparent absorbance, $\kappa_\nu + (1 - R_\nu)/d$ (with $d = 45.5$ cm), which is recorded as a function of wavelength. Wavelength variations in the mirror reflectivity R_ν or cavity alignment manifest themselves as variations in the base line. Most of the data were taken at 295 K and 950 mbar pressure of pure O_2.

The laser spectral width of about 0.5 cm^{-1} is much larger than the approximate value of 0.08 cm^{-1} that might be appropriate for our pressure conditions. Although the time histories appear to be exponential as far as $t = 6\tau$, the extracted slope still depends somewhat on the timescale included. Typically we use data only for $t \leq 3\tau$, weighted by the original signal value. Thus the value of τ is determined predominantly by the first part of the ring-down transient. Data taken at other pressures and with different focusing conditions also confirm that the mismatch of linewidths leads to non-Beer's-law behavior. The result is that the intensities of strong peaks are underestimated. The data presented here have been adjusted using a trial model

based on simulating the change in the spectral content in the laser beam resulting from a narrower absorption profile. The "strong" peaks in the data (1.15×10^{-4} cm^{-1}) have been increased by 38%, while peaks of half this strength have been increased by only 16%. These nonlinear adjustments bring the data taken at different pressures into better agreement, but indicate that the absorption strengths derived from this data may be underestimates of the actual value. All the CRDS data used in this work have been modified as just described.

3. Theoretical methods

3.1. Rotational branch intensities for forbidden transitions

Forbidden transitions are often said to "borrow" intensity from allowed transitions through spin-orbit or other coupling mechanisms. More rigorously, we express the wave function of a state as a superposition of an unperturbed component and a number of (presumably much smaller) contributions from other states admixed by the "perturbations." For example, we might represent the F_k component of the state called β by

$$\psi_{J'M}^{\beta k} = \sum_{\Lambda'\Sigma'} C_{\Lambda'\Sigma'}^{\beta k J'} \left[|\beta\Lambda'\Sigma'J'\Omega'M\rangle + \sum_{\sigma\Lambda\Sigma} |\sigma\Lambda\Sigma J'\Omega M\rangle \frac{\langle\sigma\Lambda\Sigma J'\Omega|H|\beta\Lambda'\Sigma'J'\Omega'\rangle}{E_\sigma - E_\beta} \right] \tag{2}$$

where the unperturbed basis set is the Hund's Case (a) representation $|\beta\Lambda\Sigma J\Omega M\rangle$ and the coefficients $C_{\Lambda\Sigma}^{\beta k J}$ are the spin-rotation eigencoefficients that diagonalize the matrix Hamiltonian $\langle\beta\Lambda'\Sigma'J\Omega'|H|\beta\Lambda\Sigma J\Omega\rangle$. We will suppose that the energy denominators are sufficiently large that their dependence on Λ, Σ, and J can be ignored.

The electric-dipole transition matrix element between upper state $\psi_{J'M'}^{\beta k}$ and lower state $\psi_{J''M''}^{\alpha i}$ is then

$$\langle\psi_{J'M'}^{\beta k}|\boldsymbol{\mu}|\psi_{J''M''}^{\alpha i}\rangle = \sum_{\Lambda'\Sigma'} (C_{\Lambda'\Sigma'}^{\beta k J'})^* \sum_{\Lambda''\Sigma''} C_{\Lambda''\Sigma''}^{\alpha i J''} \sum_{\sigma\Lambda} \left[\langle\beta\Lambda'\Sigma'J'\Omega'M'|\boldsymbol{\mu}|\sigma\Lambda\Sigma'J''\Omega M''\rangle \frac{\langle\sigma\Lambda\Sigma'J''\Omega|H|\alpha\Lambda''\Sigma''J''\Omega''\rangle}{E_\sigma - E_\alpha} \right.$$

$$\left. + \frac{\langle\beta\Lambda'\Sigma'J'\Omega'|H|\sigma\Lambda\Sigma''J'\Omega\rangle}{E_\sigma - E_\beta} \langle\sigma\Lambda\Sigma''J'\Omega M'|\boldsymbol{\mu}|\alpha\Lambda''\Sigma''J''\Omega''M''\rangle \right] \tag{3}$$

where we have supposed that the dipole matrix element vanishes between the unperturbed states (and between Hund's case (a) states with different values of Σ), and that the mixing of the perturbing states is sufficiently weak that we can ignore transitions from perturbations of the upper state to perturbations of the lower state.

In practical terms, the above expression can be represented as a matrix summation, with the numbers of rows and columns equal to the number of basis functions or components in the upper and lower state, respectively. The mechanistic formulation of this matrix allows us to estimate the relative sizes of the matrix elements, assuming specific types or symmetries of perturbing levels. In general, the dipole operator allows nonzero values of $\langle\beta\Lambda'\Sigma'J'\Omega'M'|\boldsymbol{\mu}|\sigma\Lambda\Sigma'J''\Omega M''\rangle$ only for $\Delta\Omega = 0, \pm 1$. For perturbations involving different spins, we assert that $\langle\sigma\Lambda\Sigma'J''\Omega|H|\alpha\Lambda''\Sigma''J''\Omega''\rangle$ will vanish if $\Delta\Omega \neq 0$, while for perturbations involving the same spin, we allow connections mediated by the rotational kinetic energy (L-uncoupling) and thus also permit $\Delta\Omega = \pm 1$. Under the assumption of unpolarized light or of unaligned molecules and the absence of electric fields, we can write a very flexible and general expression for dipole matrix elements in the form

$$\langle\psi_{J'M'}^{\beta k}|\boldsymbol{\mu}|\psi_{J''M''}^{\alpha i}\rangle = \sum_{\Lambda'\Sigma'} (C_{\Lambda'\Sigma'}^{\beta k J'})^* \sum_{\Lambda''\Sigma''} C_{\Lambda''\Sigma''}^{\alpha i J''} \left[\mu_{\Lambda'\Sigma'\Omega''\Sigma''}^{\beta\alpha(0)} S(J', \Omega', J'', \Omega'') + \mu_{\Lambda'\Sigma'\Omega''\Sigma''}^{\beta\alpha(+1)} [J(J+1) - \Omega''(\Omega''+1)]^{1/2} \right.$$

$$\left. \times S(J', \Omega', J'', \Omega''+1) + \mu_{\Lambda'\Sigma'\Omega''\Sigma''}^{\beta\alpha(-1)} [J(J+1) - \Omega''(\Omega''-1)]^{1/2} S(J', \Omega', J'', \Omega''-1) \right] \tag{4}$$

where $S(J',\Omega',J'',\Omega'')$ is the unsquared, that is signed, Hönl–London factor (refs. 41 and 42, Table 7, page 39), which we normalized such that $S(J-1, 0, J, 0) = \sqrt{J}$.

This representation can be used for any transition, including allowed ones. We suggest that the present notation is superior to the equivalent X_i, Y_i, and Z_i notation used by Kerr and Watson [22] and Lewis and Gibson [12] because it is more transparent, provides straightforward symmetry relations, is less subject to assumptions about the origin of the transition moment, and is much easier to program. The $\mu_{\Omega'\Omega''}^{(i)}$ transition-moment coefficients can be determined from a model of the transition, or treated as empirical parameters to be derived from fitting the experimental intensities, under the sign conventions that can be derived from symmetry operations that reverse the sign of the internal angular momentum projection [42]:

$$\mu_{-\Omega'-\Omega''}^{(i)} = \eta(-1)^{\Omega'-\Omega''+i} \mu_{\Omega'\Omega''}^{(i)} \tag{5}$$

TABLE 2. Comparison of branch intensity models for the 10–0 $K = 13$ Herzberg I ($A^3\Sigma_u^+ \leftarrow X^3\Sigma_g^-$) transition: columns 2–5 based on the work of Huestis and Slanger [11], column 6 from Herzberg [8], column 7 from Lewis and Gibson [12], and column 8 from Cann and Nicholls [13]

Branch	$^3\Pi_g$	Rotation	$^3\Sigma_u^-$	Total	Herzberg	Lewis and Gibson	Cann and Nicholls
$^QQ_1$	1.44	0.68	0.09	4.96	5	1.55	4.82
$^QQ_2$	0	0.66	0.19	0.74	1.5	0.04	1.46
$^QQ_3$	−1.33	0.63	0.08	0.38	1	1.14	0.97
$^QP_{32}$	0.83	−0.05	1.01	3.21	4	3.38	3.92
$^QR_{12}$	0.57	−0.05	1.50	4.09	4	4.38	3.94
$^QP_{21}$	0.69	−0.05	1.30	3.76	~3	3.10	3.05
$^QR_{23}$	0.71	0.05	1.28	4.16	~3	3.03	2.99
$^OP_{12}$	−0.57	−0.01	1.47	0.79	2	0.89	1.95
$^OP_{23}$	−0.63	−0.00	1.23	0.36	0.5	0.69	0.50
$^OQ_{13}$	−0.23	0.12	0.04	0.01	0.3	0.02	0.30
$^SQ_{31}$	−0.22	−0.12	0.08	0.07		0.16	0.15
$^SR_{21}$	−0.77	0.00	1.35	0.34	0.5	0.76	0.49
$^SR_{32}$	−0.79	−0.00	1.09	0.09		0.07	0.07

The sign of $\eta = \pm 1$ is determined from the overall character of the electronic transition, and is related to the classification of levels into *e*- and *f*-parity types and to the determination of which components are involved in the rotational branches (i.e., *P*, *Q*, and *R*). For $^3\Sigma_u^+ - {}^3\Sigma_g^-$ and $^1\Sigma_u^- - {}^3\Sigma_g^-$ transitions we have $\eta = -1$.

Allowed transitions are often classified as "parallel" or "perpendicular," which means that $\mu^{(0)}_{\Omega'\Omega''}$ is nonzero only for $\Omega' - \Omega'' = 0$ or ± 1, respectively. Kopp and Hougen [43] presented the first detailed treatment of interference between parallel and perpendicular transitions for $\Omega' = \pm 1/2$ to $\Omega'' = \pm 1/2$ in which spin-orbit interactions mix $^2\Sigma_{1/2}$ and $^2\Pi_{1/2}$ characters. Some branches experience constructive and others destructive interference because the sign of $\mu^{(0)}_{\Omega'\Omega''} \times S(J', \Omega', J'', \Omega'')$ depends on both $\Delta\Omega$ and ΔJ. Carroll [44] describes a related situation in which the Σ and Π components of *np* Rydberg states of N_2 (i.e., a "*p*-complex") are strongly coupled by the rotational kinetic energy term in the Hamiltonian. In that case destructive interference extinguishes the *O*- and *S*-form branches.

3.2. The DIATOM spectral simulation computer program

The DIATOM spectral simulation computer program was developed at SRI beginning in 1980 with the specific objective of treating forbidden transitions such as the Herzberg bands. As such, it is an extension of the RLS "Rotational Line Strength" computer program written for allowed transitions by Zare and colleagues [45]. DIATOM is intended to be graphical and interactive, based on the KVS "Keyword, Value, Switch" programmable command-line interpreter and GRA graphics package, also developed at SRI. KVS and GRA run under VAX/VMS, MSDOS, and AIX/IBM-RS/6000, and on the Macintosh, and support a range of graphical displays, printers, and plotters. The DIATOM driver routines are all written in Fortran and can be converted from VAX/VMS to other platforms and operating systems. DIATOM has been used for a number of published investigations, including simulations of the absorptions and emissions of O_2 [4, 5, 10, 19, 46, 47], C_2 [48], and NO [49].

The electronic states are described by the "Brown Hamiltonian" [50], with extensions to include *L*-complexes and spin-complexes (e.g., a combination of a $^1\Pi$ and a $^3\Pi$ considered as a single electronic state). The transition moment parameters are either estimated automatically (guessing the origin of the transition moment) or else explicitly provided by the user. A variety of line-shape functions are provided. Multiple transitions can be summed under user control. For allowed transitions DIATOM and RLS are effectively equivalent, but care must be taken in converting spectroscopic constants between the "Zare Hamiltonian" [51] and the "Brown Hamiltonian," especially in the definition of the band origin (for Π states see Brown et al. [52]).

3.3. Simulation of the Herzberg bands

The spectroscopic constants used for the $A^3\Sigma_u^+$ and $c^1\Sigma_u^-$ states are derived from the work of Ramsay and co-workers [9, 16]. Constants for $X^3\Sigma_g^-$ and $A'^3\Delta_u$ come from the tabulations of Slanger and Cosby [53]. The zero of energy is chosen to be the extrapolated (nonexistent) $v'' = 0$, $J = K = 0$ level of $X^3\Sigma_g^-$. The band origins were adjusted to achieve agreement between the calculated and observed line positions. As noted by Borrell et al. [9], $v' = 11$ of $A^3\Sigma_u^+$ is perturbed. Our calculated line positions match those calculated by Borrell et al., and thus also differ by up to 2 cm^{-1} from those Borrell et al. observed.

Branch intensity parameters for $A^3\Sigma_u^+ \leftarrow X^3\Sigma_g^-$ were taken from our previous work [11]. Briefly stated, the spin-orbit contributions from $^3\Sigma_u^-$ and $^3\Pi_g$ and rotational contributions from $^3\Pi_g$ perturbers were chosen to achieve a best fit to the intensities estimated by Herzberg [8] for the 10–0 $K = 13$ lines (Herzberg's vibrational assignments were increased by one by Broida and Gaydon [1]). The resulting fit is shown in Table 2 (column 5, labeled "total" is obtained by squaring the sum of columns 2, 3, and 4). We can see that individually the three sources of transition probability contribute quite differently to the various branches, and that the resulting constructive and destructive interference gives a reasonable representation of the observed intensities. As noted by Cann and Nicholls [13], the formulas of Lewis and Gibson [12] give inferior estimates for the $^QQ_1$ and $^QQ_2$ branches. As Cann and Nicholls also note, their almost exact agreement with Herzberg's estimates is actually based on an arbitrary and empirical adjustment "without any theoretical justification" and thus does not provide the foundation for a general treatment. The simulations described in this paper are based on our 1983 parameters, supported by the excellent agreement, shown in Fig. 1, that we were able to achieve in simulating the best "graphical" spectrum we were able to find, that reported by Degen in 1968 [15]. The fact that intensity parameters derived from $\Delta v = +10$ gave a good simulation for $\Delta v = -7$ adds support for using the same parameters for all v' and v''.

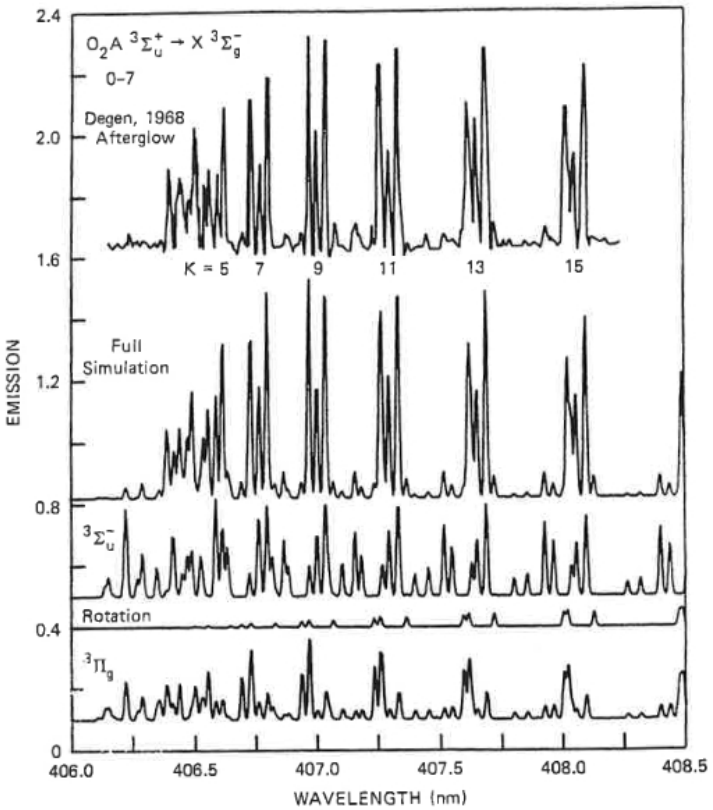

FIG. 1. Comparison of simulated spectrum [11] with afterglow emission [15], the 0–7 Herzberg I ($A^3\Sigma_u^+ \leftarrow X^3\Sigma_g^-$) transition, showing contributions of individual mechanisms.

In the notation introduced above, the transition-moment parameters are

$$\mu_{11}^{(0)} = 0.927 \tag{6}$$

$$\mu_{10}^{(0)} = \mu_{01}^{(0)} = 0.484 \tag{7}$$

$$\mu_{11}^{(1)} = \mu_{00}^{(1)} = \mu_{-1-1}^{(1)} = 0.0125 \tag{8}$$

with all others zero if not related by symmetry. The numerical values listed above are not known accurately. They are listed to three figures for definiteness. In the most general case the five parameters above can all be taken as independent, and $\mu_{10}^{(1)}$, $\mu_{0-1}^{(1)}$, and $\mu_{1-1}^{(1)}$ can also be independent and nonzero.

Branch intensity parameters for $A'^3\Delta_u \leftarrow X^3\Sigma_g^-$ are modified versions of those obtained by Kerr and Watson [22], basically choosing a single set of parameters for all v'. In the present notation the parameters are

$$\mu_{21}^{(0)} = 1.00 \tag{9}$$

$$\mu_{11}^{(0)} = 0.16 \tag{10}$$

$$\mu_{10}^{(0)} = 0.84 \tag{11}$$

$$\mu_{31}^{(1)} = 0.054 \tag{12}$$

$$\mu_{20}^{(1)} = 0.053 \tag{13}$$

$$\mu_{1-1}^{(1)} = 0.033 \tag{14}$$

once again with all others zero if not related by symmetry (with $\eta = -1$). As was the case for Herzberg I, more $\mu_{\Omega'\Omega''}^{(1)}$ parameters can be nonzero.

The $\mu_{\Omega'\Omega''}^{(i)}$ parameters described above, with maximum values approximately unity, are clearly intended to provide "relative" descriptions of the strengths of the individual rotational branches. After the overall oscillator strength of a vibrational band is known we have a choice to make about how to partition the overall transition moment into components: electronic transition moment, Franck–Condon factor, and internal branch-strength transition moment coefficients. This choice is particularly difficult for transitions with rotational contributions, since the oscillator strength will vary with rotational population, and thus with temperature and whether we are investigating emission or absorption. One possible solution is to define a standard "sum rule" for the internal branch-strength transition moment coefficients resembling that used for allowed transitions.

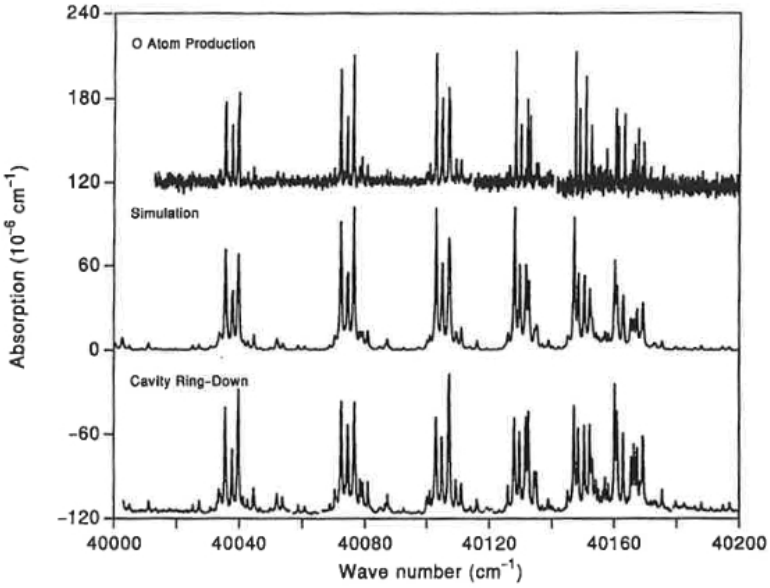

FIG. 2. O_2 absorption spectra in the vicinity of the band head of the 8–0 Herzberg I ($A^3\Sigma_u^+ \leftarrow X^3\Sigma_g^-$) transition: upper trace from O-atom production, central trace from simulation, and lower trace from cavity ring-down absorption.

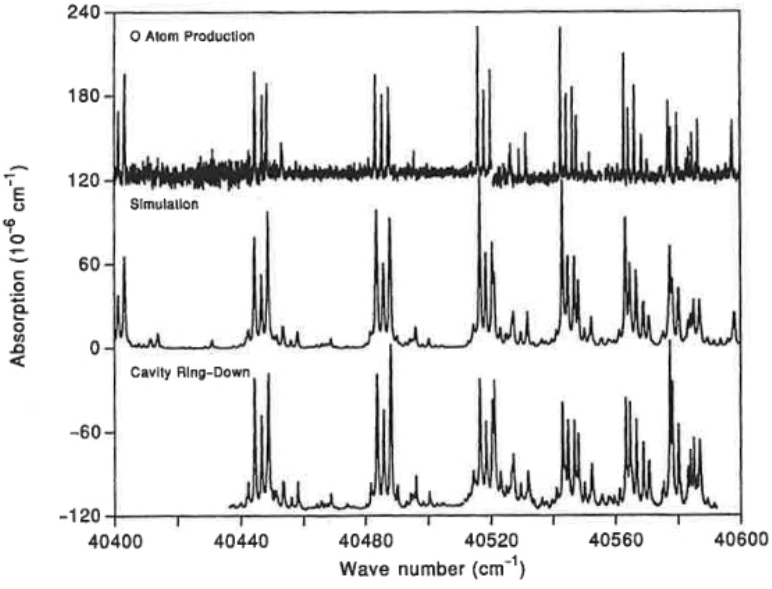

FIG. 3. O_2 absorption spectra in the vicinity of the band head of the 9–0 Herzberg I ($A^3\Sigma_u^+ \leftarrow X^3\Sigma_g^-$) transition: upper trace from O-atom production, central trace from simulation, and lower trace from cavity ring-down absorption.

4. Results and discussion

Figures 2–5 show the experimental absorption spectra and spectral simulations in the regions of the band heads of the 8–0, 9–0, 10–0, and 11–0 vibrational bands of the Herzberg I system ($A^3\Sigma_u^+ \leftarrow X^3\Sigma_g^-$). In each figure the lower trace shows the nominally absolute absorption spectrum from the cavity ring-down experiments, with a background subtracted of approximately 1.1×10^{-4} cm^{-1} due to cavity mirror losses, adjusted upward in amplitude as described above, and shifted downward for display. The upper traces come from the O-atom production experiments, adjusted in amplitude for each scan for internal consistency between overlapping scans and to best match the peak heights of the simulation, and shifted upward for display.

The central traces show the simulated absorption spectra. We have used the branch-strength formulas described above, based for Herzberg I on Huestis and Slanger [11] and for Herzberg III on Kerr and Watson [22]. The relative intensities of the vibrational

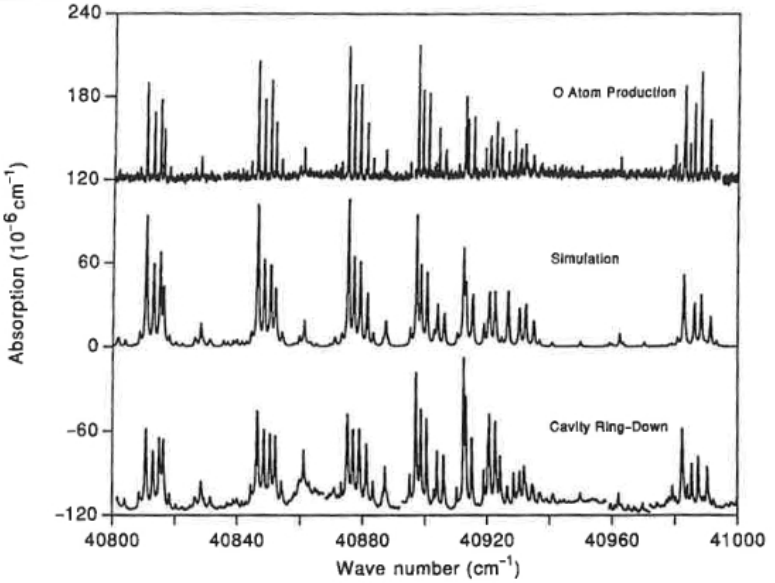

FIG. 4. O_2 absorption spectra in the vicinity of the band head of the 10–0 Herzberg I ($A^3\Sigma_u^+ \leftarrow X^3\Sigma_g^-$) transition: upper trace from O-atom production, central trace from simulation, and lower trace from cavity ring-down absorption.

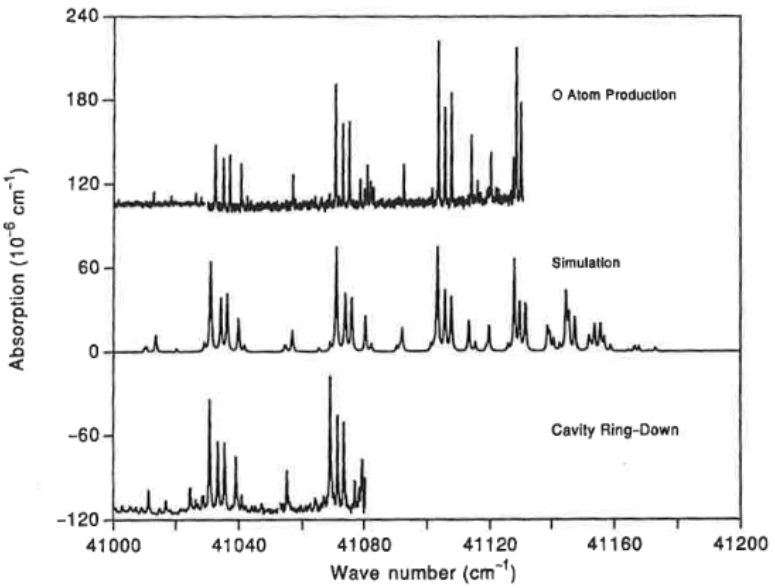

FIG. 5. O_2 absorption spectra in the vicinity of the band head of the 11–0 Herzberg I ($A^3\Sigma_u^+ \leftarrow X^3\Sigma_g^-$) transition: upper trace from O-atom production, central trace from simulation, and lower trace from cavity ring-down absorption.

bands are determined purely from Franck–Condon factors, that is, assuming R-independent transition moments, in disagreement with the calculated transition moments of Klotz and Peyerimhoff [28], although the limited range of v' explored is probably not sufficient to expose any R-dependence. Franck–Condon factors for Herzberg I have been taken from Krupenie [54] (they were actually calculated in 1968 by W.R. Jarmain and published by Degen and Nicholls [24]). Franck–Condon factors for Herzberg II and III were calculated for us by Albritton,[2] and extended for Herzberg II to higher vibrational levels in the Morse-oscillator approximation. Thus there are only three free parameters in the simulation, the absorption strengths of the three band systems: Herzberg I, II, and III. How these are determined will be described below.

Overall, the agreements between the two experiments, between the experiments and the simulation, and between the present work and the data published by Wildt et al. [32] are

[2]D.L. Albritton. Private communication, 1979.

TABLE 3. Oscillator strengths for Herzberg I ($A^3\Sigma_u^+ - X^3\Sigma_g^-$): HND70, emission calibrated against 7–0 absorption band (Hasson, Nicholls, and Degen [25]); HN71, absorption (Hasson and Nicholls [26]); Ba89, theory (Bates [29]); CRDS, cavity ring-down spectroscopy (present work); and Recommended, frequency times Franck–Condon factor normalized at 7–0 (present work, estimated uncertainty 15%)

$v'-v''$	HND70	HN71	Ba89	CRDS	Recommended
0–0	8.53–14	—	1.35–13	—	1.06–13
1–0	7.45–13	—	1.11–12	—	8.91–13
2–0	3.33–12	—	4.83–12	—	3.85–12
3–0	1.03–11	—	1.51–11	—	1.14–11
4–0	2.46–11	3.00–11	3.44–11	—	2.66–11
5–0	4.88–11	5.38–11	6.86–11	—	5.14–11
6–0	8.34–11	7.98–11	1.17–10	—	8.58–11
7–0	1.24–10	1.24–10	1.71–10	—	1.24–10
8–0	1.63–10	1.39–10	2.23–10	8.80–11	1.60–10
9–0	1.85–10	1.40–10	2.64–10	1.08–10	1.78–10
10–0	1.77–10	1.20–10	2.42–10	9.30–11	1.68–10
11–0	1.25–10	1.00–10	8.40–11	6.80–11	9.93–11*

*At 295 K 84% of the nominal value.

extremely good. All the strong features are Herzberg I transitions. The details of relative strengths of the strong features vary. In some cases the simulation looks more like one of the experiments, while for the next value of K it looks more like the other one. Some of these differences could be due to choice of the simulation lineshape (Lorentzian of 0.55 cm^{-1} width) and some could be due to finite experimental sampling missing the peak absorption. Both experiments show 10–20% variations in the relative intensities of the strong peaks as determined from multiple scans over the same wavelength region.

One consistent difference is that the cavity ring-down experiments show a maximum intensity at $K = 3$ for all bands. On the other hand, the O-atom production experiments, the simulation, and the data of Wildt et al. show maxima for $K = 5$ or $K = 7$. We believe that this disagreement is caused by experimental details in the CRDS experiments that we do not understand, but are related to the non-Beer's-law behavior.

Another difference is that the weak features in the cavity ring-down spectra are consistently stronger, relative to the main Herzberg I peaks, than in the O-atom production, the simulated spectra, or the data of Wildt et al. Some of these weak features are due to Herzberg II and Herzberg III, and could have a lower yield of oxygen atoms. This could explain why some of the weak features might be missing from O-atom production spectra. However, most of the weak peaks in the O-atom production spectra are assigned as Herzberg I absorption lines, and should have the same O-atom yield as the strong peaks involving the same upper states. The most probable explanation is that we have not yet adequately compensated for non-Beer's-law behavior in the cavity ring-down experiments. We conclude, supported by the discussion of oscillator strengths below, that the weak peaks are more likely to be correct and that, even after our attempts at adjustment and correction, the strong peaks remain diminished by the experimental conditions of the cavity ring-down experiments. Similar quibbles over details can be applied to the data of Wildt et al. For example, we do not understand why Wildt et al. observe the c–X 13–0 $^RQ(7)$ and $^QR(7)$ lines at 40 051.7 and 40 053.7 cm^{-1} but not the $^PP(5)$ and $^PQ(5)$ lines at 40 058.5 and 40 060.6 cm^{-1}.

The good agreement between the simulation and the data from O-atom production and from Wildt et al. leads us to reject the possible interpretation that the simulation is underestimating the intensities of the weak features. It is indeed the case that we had hoped to improve the Herzberg I branch intensity formulas by fitting the spectra, but have concluded that the agreement is already comparable to the scan-to-scan variation in the experiments. The principal remaining shortcoming of the simulation is that the relative intensity of the leftmost strong peak, $^QR_{23} + {}^QP_{21}$, is consistently predicted to be stronger than experimentally observed for small K.

The simulation of the Herzberg I bands was normalized to the cavity ring-down data by equating the areas over the central peaks of the 10–0, $K = 9$ transition, and then choosing the simulation linewidth of 0.55 cm^{-1} to give a good representation of the peak intensities. Inspection of Figs. 2–5 suggests that this produces an adequate normalization for all the vibrational bands investigated. Subsequently, we compute the ratios of the areas of the cavity ring-down and simulated spectra over the central peaks of the 8–0, $K = 13$ and $K = 15$; 9–0, $K = 11$ and $K = 13$; and 11–0, $K = 9$ and $K = 11$ transitions. The relative values obtained are 0.98 ± 0.02, 1.08 ± 0.02, and 1.22 ± 0.04, for 8–0, 9–0, and 11–0, respectively (the uncertainty limits indicate the spread of the values obtained from the two K values inspected in each case). Since the above normalization places the simulation on an absolute scale, oscillator strengths for each vibrational band were then obtained by integrating the simulated absorption cross section for that band, and multiplying by the relative values just obtained (see Steinfeld [55] p. 28–29, for a useful summary of radiation formulas). Integrating the simulation is superior to integrating the experimental spectrum directly because the former isolates the multiple overlapping electronic transitions and vibrational bands. The results are listed in the fifth column of Table 3.

Also shown in Table 3 are the three other determinations of the oscillator strengths for Herzberg I (where we have converted from linestrength, $S_{v'v''}$, or Einstein coefficient, $A_{v'v''}$, as necessary). The cavity ring-down determinations are significantly lower, and the calculations significantly higher than the others, but there is sufficient disagreement that it is not obvious which values to prefer. To select the most appropriate we will use the one additional piece of information available, the cross section for the Herzberg continuum. There have been a number of measurements of the Herzberg continuum cross section, the latest by Yoshino et al. [27]. Saxon and Slanger [30] also

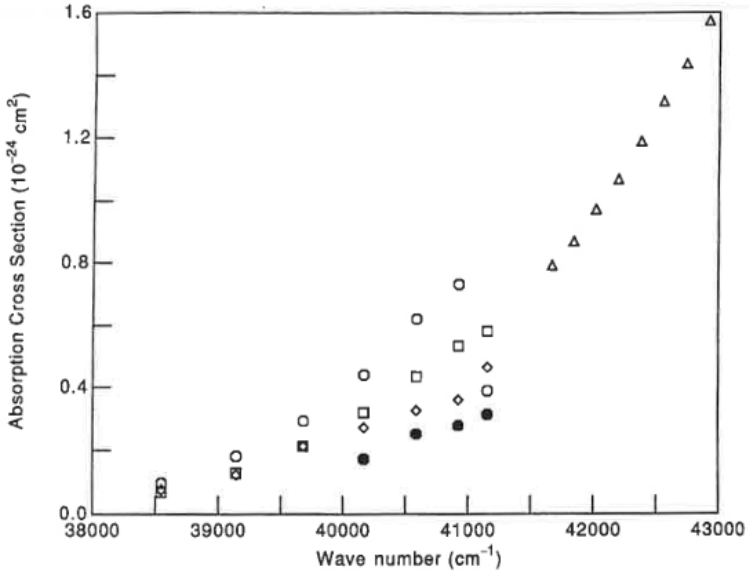

FIG. 6. Graph of effective absorption cross sections for Herzberg I continuum (triangles, from Yoshino et al. [27]) and bound–bound transitions, comparing Bates (open circles, [29]), Nicholls and colleagues (squares [25] and diamonds [26]), and present work (filled circles, CRDS).

calculated it based on the transition moments of Klotz and Peyerimhoff [28]. They found a similar shape for the continua from Herzberg I, II, and III, and estimated, based on the theoretical transition moments [28], that about 70% of the continuum cross section comes from Herzberg I. In the discussion below, we will lower the relative strength of the Herzberg II and Herzberg III transitions, and suggest the new estimate for Herzberg I continuum as about 86% of the total.

We use the concept of "continuity" of the integrated absorption cross section across the dissociation limit as a means of comparing and choosing between different sources of the absorption strengths for at least the highest A–X $v' = 0$ bands. The correctness of this procedure has been demonstrated on the Schumann–Runge bands by several authors (Allison and Dalgarno, [56]; Saxon and Slanger [57]). The absorption cross section for the continuum is related to the absorption f-number for a nearby band by the expression [57]

$$\sigma(E) \approx 8.85 \times 10^{-13} f_{v'0}\, \rho(E) \qquad (15)$$

where $\rho(E)$ is the density of states (in cm), or the reciprocal of the vibrational level spacing, appropriately averaged. Figure 6 shows a limited range of the Herzberg continuum cross section (multiplied by 0.86, triangles), the derived effective cross sections from the 5–0, 6–0, 7–0, 8–0, 9–0, 10–0, and 11–0 Herzberg I vibrational bands, using the oscillator strengths from the emission modeling of Hasson et al. [25] (squares), direct experimental determinations by Hasson and Nicholls [26] (diamonds), calculations by Bates [29] (open circles), and cavity ring-down experiments (filled circles). While one might argue about the details, the vibrational-band data of Hasson et al. [25] are clearly consistent with the continuum cross section. Surprisingly, the direct absorption measurements of Hasson and Nicholls [26] are slightly low for $v' > 7$ (but perhaps not completely inconsistent with the continuum cross section). We are also surprised that Hasson and Nicholls did not compare and discuss the two works from their own laboratory. Hasson et al. do not have any actual experimental data for $v' = 9$–11 and all of the emission intensities are normalized to the single absorption cross section (7–0) shared between the two works. Bates' calculations are too high (except for his anomalous $v' = 11$) and the present cavity ring-down experiments appear too low, although both have the right shape.

In any case, we now have a consistent normalization for the Herzberg I oscillator strengths. One choice is to accept the tabular values, or some average of Hasson et al. [25] and Hasson and Nicolls [26]. We prefer to use the somewhat simpler approach (i.e., simpler to implement in a computer program) of accepting the Franck–Condon factors as representing the relative transition strengths, and normalizing everything to the value of 1.24×10^{-10} for the 7–0 band, given in column 6 as "Recommended" in Table 3. The absorption oscillator strength for the 11–0 band needs to be adjusted explicitly since about 16% (at 295 K) of the transition probability from the ground state would be associated with K' levels higher than those observed above the dissociation limit (41 267.5 ± 1.0 cm^{-1} [58]). About 2% of the 10–0 transition probability also belongs to the continuum. To be consistent with the recommended values, Bates' values [29] must be multiplied by a factor of 0.7, suggesting that the magnitude of the transition moment is overestimated by Klotz and Peyerimhoff [28], and the present cavity ring-down values should be multiplied by a factor of 1.75, suggesting that we have not yet corrected adequately the observed experimental absorptions.

Review of Figs. 2–5 shows that the simulation and cavity ring-down spectra contain numerous small peaks, the strongest of which can be assigned to Herzberg I, but the majority of which come from Herzberg II and III. The intensities of the Herzberg II and III features were simulated by eyeball comparisons with the weak Herzberg I features in the same spectral regions (i.e., assuming that the simulation calculates the intensities of weak Herzberg I lines correctly, supported by the

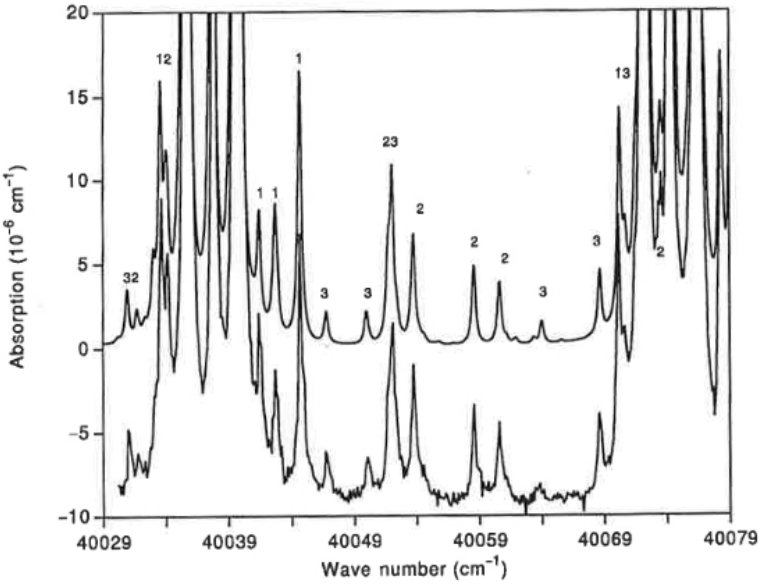

FIG. 7. Expansion of absorption spectrum from Fig. 2, illustrating Herzberg II ($c^1\Sigma_u^- \leftarrow X^3\Sigma_g^-$) (labeled with "2") and Herzberg III ($A'^3\Delta_u \leftarrow X^3\Sigma_g^-$) (labeled with "3") transitions. Some of the weaker Herzberg I ($A^3\Sigma_u^+ \leftarrow X^3\Sigma_g^-$) are labled with "1". The lower trace is from the cavity ring-down experiments and the upper trace from the simulation.

TABLE 4. Oscillator strengths for Herzberg II ($c^1\Sigma_u^- - X^3\Sigma_g^-$): Ba89, theory (Bates [29]); CRDS, cavity ring-down spectroscopy (present work); and Recommended, frequency times Franck–Condon factor normalized over 13–0, 14–0, 16–0 (present work, estimated uncertainty 30%)

$v'-v''$	Ba89	CRDS	Recommended
10–0	1.81–11	—	3.94–12
11–0	2.10–11	—	4.82–12
12–0	2.37–11	—	5.68–12
13–0	2.49–11	7.02–12	6.43–12
14–0	2.48–11	6.61–12	7.09–12
15–0	2.36–11	—	7.56–12
16–0	2.39–11	8.38–12	7.85–12

TABLE 5. Oscillator Strengths for Herzberg III ($A'^3\Delta_u - X^3\Sigma_g^-$): Ba89, theory (Bates [29]); CRDS, cavity ring-down spectroscopy (present work); and Recommended, frequency times Franck–Condon factor normalized to 9–0 (present work, estimated uncertainty 30%)

$v'-v''$	Ba89	CRDS	Recommended
6–0	3.02–11	—	8.40–12
7–0	4.49–11	—	1.25–11
8–0	6.28–11	—	1.64–11
9–0	7.62–11	1.92–11	1.92–11
10–0	8.39–11	—	2.02–11
11–0	8.08–11	1.67–11	1.67–11

comparison discussed above with the O-atom production data and that of Wildt et al. [32]). Figure 7 shows an expansion taken from Fig. 2 (in which the simulation is now performed with a Lorentzian width of 0.35 cm^{-1}, which will make the strong peaks 57% taller than ones from the cavity ring-down experiment, comparable to the 75% increase suggested above). Clearly, the simulation is doing very well, with everything explained quantitatively down to the signal-to-noise limit of the experiment (this scan can be compared to one in the same region by Wildt et al. [32]). Similar quality-of-fit is obtained over the other spectral regions examined in detail (40 150–40 200, 40 240–40 320, and 40 800–40 870 cm^{-1}). In addition, there are a number of weak peaks in the cavity ring-down spectrum between 40 900 and 41 080 cm^{-1} that are not present in the simulation. Some of these lines are due to the previously unreported 17–0 Herzberg II and 12–0 Herzberg III bands (to be reported separately), but other relatively strong lines, notably at 40 980.0 and 40 984.8 cm^{-1} in Fig. 4 and clustered around 41 080 cm^{-1} in Fig. 5, are not obviously associated with any of the three systems. They were not reported by Herzberg [8] or Borrell et al. [9], yet are quite evident both in the O-atom spectra and in the CRD spectra. Yoshino et al. [59] discuss perturbations in the A–X 11–0 region, which they suggest may be due to involvement of the $^3\Pi_u$ state. We have found about 20 lines in the 40 930–41 080 cm^{-1} range in the CRD spectra that have not previously been listed, and do not belong to the two new bands.

By integrating the simulated Herzberg II and Herzberg III vibrational bands we can obtain oscillator strengths relative to the Herzberg I bands to which they have been normalized. The results are shown in column 3 of Tables 4 and 5. The normalization has been done relative to the Recommended values of the Herzberg I oscillator strengths in Table 3. The only extensive information available for comparison is the calculations of Bates [29], shown in column 2 of Tables 4 and 5. The conversion of Bates' (emission) Einstein coefficients for Herzberg III into (absorption) oscillator strengths depends on the assumed Ω' population (which Bates assumed to be equal) and on assignment of the effective excited-state degeneracy (which we

take to be 6). For both the Herzberg II and Herzberg III transitions, Tables 4 and 5 show that Bates' numbers appear to be about 4 times too large. In both Tables 4 and 5 the column labeled Recommended corresponds to the Franck–Condon factors we have used (times frequency, normalized to the CRDS data), except for the 11–0 band of Herzberg III, for which we do not have a calculated Franck–Condon factor.

The estimate used above, that 86% of the Herzberg continuum comes from Herzberg I, can now be justified by comparing the oscillator strengths for three bands, 8–0, 13–0, and 9–0, for Herzberg I, II, and III, that occur in the same spectral region. Finally, we can compare the ratios of the oscillator strengths for the 10–0 Herzberg II and 6–0 Herzberg I bands. We find the Herzberg I band to be 22 times stronger, in satisfactory agreement with the qualitative estimate of 30 times, from Hasson and Nicholls [26].

5. Conclusions

The experimental data presented here provide strong support for the theoretical models of the branch intensities of the Herzberg I ($A^3\Sigma_u^+ \leftarrow X^3\Sigma_g^-$) and Herzberg III ($A'^3\Delta_u \leftarrow X^3\Sigma_g^-$) transitions. The cavity ring-down spectroscopy data provide the first direct experimental information about the oscillator strengths of the Herzberg II ($c^1\Sigma_u^- \leftarrow X^3\Sigma_g^-$) and Herzberg III transitions. The data presented here are combined with those available in the literature to provide Recommended oscillator strengths for all three transitions.

NOTE ADDED IN PROOF: In an upcoming paper we will combine the absorption data described here with any available information on the emissions from the three Herzberg upper levels to estimate Einstein coefficients. We have calculated new Franck–Condon factors for Herzberg II and III, which will lead to changes in vibrational-level dependence of the recommended oscillator strengths for these two systems.

Acknowledgements

The work at SRI was supported by the U.S. National Science Foundation (Atmospheric Chemistry Program) and the U.S. National Aeronautics and Space Administration (Stratospheric Chemistry Section). The oxygen-atom detection experiments at SRI were supported by the U.S. Air Force Electronics Systems Center and the U.S. Air Force Phillips Laboratory (Contract No. F19628-93-C-0178). The simulations and data analysis were performed on a Digital Equipment Corporation VAX 11/750 computer purchased under NSF grant No. PHY-8114611. The work at the University of Nijmegen is part of the research program of the "Stichting voor Fundamenteel Onderzoek der Materie (FOM)," which is financially supported by the "Nederlandse Organisatie vor Wetenschappelijk Onderzoek (NWO)."

1. H.P. Broida and A.G. Gaydon. Proc. R. Soc. (London), A, **222**, 181 (1954).
2. A.L. Broadfoot and K.R. Kendall. J. Geophys. Res. **73**, 426 (1968).
3. V. Degen. J. Geophys. Res. **74**, 5145 (1969).
4. T.G. Slanger and D.L. Huestis. J. Geophys. Res. **86**, 3351 (1981).
5. T.G. Slanger and D.L. Huestis. J. Geophys. Res. **88**, 4137 (1983).
6. G. Herzberg. Naturwissenschaften, **20**, 577 (1932).
7. R.D. Present. Phys. Rev. **48**, 140 (1935).
8. G. Herzberg. Can. J. Phys. **30**, 185 (1952).
9. P.M. Borrell, P. Borrell, and D.A. Ramsay. Can. J. Phys. **64**, 721 (1986).
10. T.G. Slanger and D.L. Huestis. J. Chem. Phys. **78**, 2274 (1983).
11. D.L. Huestis and T.G. Slanger. 38th Symp. Mol. Spectrosc. Columbus, Ohio, June 1983.
12. B.R. Lewis and S.T. Gibson. Can. J. Phys. **68**, 231 (1990).
13. M.W.P. Cann and R. Nicholls. Can. J. Phys. **69**, 1163 (1991).
14. G. Herzberg. Can. J. Phys. **31**, 657 (1953).
15. V. Degen. Can. J. Phys. **46**, 784 (1968).
16. D.A. Ramsay. Can. J. Phys. **64**, 717 (1986).
17. G.M. Lawrence, C.A. Barth, and V. Argabright. Science, **195**, 537 (1977).
18. T.G. Slanger. J. Chem. Phys. **69**, 4779 (1978).
19. T.G. Slanger and V. Degen. Planet. Space Sci. **34**, 971 (1986).
20. V.A. Krasnopol'skii, A.A. Krys'ko, V.N. Pogashcv, and V.A. Parshev. Cosmic Res. (Engl. Transl.), **13**, 687 (1977).
21. T.G. Slanger and G. Black. Geophys. Res. Lett. **5**, 947 (1978).
22. C.M.L. Kerr and J.K.G. Watson. Can. J. Phys. **64**, 36 (1986).
23. B. Coquart and D.A. Ramsay. Can. J. Phys. **64**, 726 (1986).
24. V. Degen and R.W. Nicholls. J. Phys. B: At. Mol. Phys. **2**, 1240 (1969).
25. V. Hasson, R.W. Nicholls, and V. Degen. J. Phys. B: At. Mol. Phys. **3**, 1192 (1970).
26. V. Hasson and R.W. Nicholls. J. Phys. B: At. Mol. Phys. **4**, 1178 (1971).
27. K. Yoshino, J.R. Esmond, A.S.-C. Cheung, D.E. Freeman, and W.H. Parkinson. Planet. Space Sci. **40**, 185 (1992).
28. R. Klotz and S.D. Peyerimhoff. Mol. Phys. **57**, 573 (1986).
29. D.R. Bates. Planet. Space Sci. **37**, 881 (1989).
30. R.P. Saxon and T.G. Slanger. J. Geophys. Res. **91**, 9877 (1986).
31. A.S.-C. Cheung, K. Yoshino, W.H. Parkinson, S.L. Guberman, and D.E. Freeman. Planet. Space Sci. **34**, 1007 (1986).
32. J. Wildt, G. Bednarek, E.H. Fink, and R.P. Wayne. Chem. Phys. **156**, 497 (1991).
33. R.A. Copeland, K. Knutsen, and T.G. Slanger. Proc. Int. Conf. Lasers '93, Society for Optical and Quantum Electronics, McLean, Va. In press. 1994.
34. W.K. Bischel, B.E. Perry, and D.R. Crosley. Chem. Phys. Lett. **82**, 85 (1981).
35. D.J. Bamford, L.E. Jusinski, and W.K. Bischel. Phys. Rev. A: Gen. Phys. **34**, 185 (1986).
36. A. O'Keefe and D.A.G. Deacon. Rev. Sci. Instrum. **59**, 2544 (1988).
37. A. O'Keefe, J.J. Scherer, A.L. Cooksy, R. Sheeks, J. Heath, and R. Saykally. Chem. Phys. Lett. **172**, 214 (1990).
38. D. Romanini and K.K. Lehmann. J. Chem. Phys. **99**, 6287 (1993).
39. G. Meijer, M.G.H. Boogaarts, R.T. Jogma, D.H. Parker, and A.M. Wodtke. Chem. Phys. Lett. **217**, 112 (1994).
40. R.T. Jongma, M.G.H. Boogarts, and G. Meijer. J. Mol. Spectrosc. **165**, 303 (1994).
41. H. Hönl and F. London. Z. Phys. **33**, 803 (1925).
42. J.T. Hougen. The calculation of rotational energy levels and line intensities in diatomic molecules. N.B.S. Standards Monogr. (U.S.) **115**, (1970).
43. I. Kopp and J.T. Hougen. Can. J. Phys. **45**, 2581 (1967).
44. P.K. Carroll. J. Chem. Phys. **58**, 3597 (1973).
45. R.N. Zare. *In* Molecular spectroscopy: modern research. *Edited by* K.N. Rao and C.W. Mathews. Academic Press, New York. 1972. Chap. 4.
46. J. Stegman and D.P. Murtagh. Planet. Space Sci. **36**, 927 (1988).
47. J. Stegman and D.P. Murtagh. Planet. Space Sci. **39**, 595 (1991).
48. K.R. Stalder and R.L. Sharpless. J. Appl. Phys. **68**, 6187 (1990).
49. M.J. Dyer, G.W. Faris, P.C. Cosby, D.L. Huestis, and T.G. Slanger. Chem. Phys. **171**, 237 (1993).
50. J.M. Brown and A.J. Merer. J. Mol. Spectrosc. **74**, 488 (1979).
51. R.N. Zare, A.L. Schmeltekopf, W.J. Harrop, and D.L. Albritton. J. Mol. Spectrosc. **46**, 37 (1973).
52. J.M. Brown, E.A. Colburn, J.K.G. Watson, and F.D. Wayne. J. Mol. Spectrosc. **74**, 294 (1979).

53. T.G. Slanger and P.C. Cosby. J. Phys. Chem. **92**, 267 (1988).
54. P.H. Krupenie. J. Phys. Chem. Ref. Data, **1**, 423 (1970).
55. J.I. Steinfeld. Molecules and radiation. Harper & Row, New York. 1974.
56. A.C. Allison and A. Dalgarno. J. Chem. Phys. **55**, 4342 (1971).
57. R.P. Saxon and T.G. Slanger. J. Geophys. Res. **96**, 17291 (1991).
58. P.C. Cosby and D.L. Huestis. J. Chem. Phys. **97**, 6108 (1992).
59. K. Yoshino, J.E. Murray, J.R. Esmond, Y. Sun, W.H. Parkinson, A.P. Thorne, R.G.M. Learner, and G. Cox. Can. J. Phys. **72**, 1101 (1994).